Sensors and Actuators B 250 (2017) 402–411

Contents lists available at ScienceDirect

Sensors and Actuators B: Chemical

journal homepage: www.elsevier.com/locate/snb

High-fidelity bioelectronic muscular actuator based on porous carboxylate bacterial cellulose membrane

Fan Wang[a], Zhen Jin[a], Shaohui Zheng[a], Hao Li[a], Sunghoon Cho[a], Hyeon Joe Kim[b], Seong-Jun Kim[b], Eunpyo Choi[a], Jong-Oh Park[a,*], Sukho Park[a,c,*]

[a] School of Mechanical Engineering, Chonnam National University, 77 Yongbong-ro, Buk-gu, Gwangju 500-757, Republic of Korea
[b] Department of Environmental Engineering, Chonnam National University, 77 Yongbong-ro, Buk-gu, Gwangju 500-757, Republic of Korea
[c] Department of Robotics Engineering, Daegu Gyeongbuk Institute of Science and Technology, Daegu, 711-873, Republic of Korea

ARTICLE INFO

Article history:
Received 23 February 2017
Received in revised form 13 April 2017
Accepted 20 April 2017
Available online 27 April 2017

Keywords:
Eco-friendly
Actuator
Porous
Carboxylate bacterial cellulose

ABSTRACT

Human-friendly electronic products, such as smart mobile phones, soft haptic devices, wearable electronics, and implantable or disposal biomedical devices, will require the use of high-performance durable soft electroactive actuators with eco-friendly, biocompatible, and biodegradable functionalities. Here, we report a high-fidelity bioelectronic muscular actuator based on porous carboxylate bacterial cellulose (CBC) membranes fabricated using the facile zinc oxide (ZnO) particulate leaching (PL) method. The proposed CZ-PL muscular actuator exhibits large deformation, low actuation voltage, fast response, and high-durability in open air environment. In particular, the CZ-PL membrane shows a dramatic increase in the ionic liquid uptake ratio, ionic exchange capacity, and ionic conductivity of up to 70.63%, 22.50%, and 18.2%, respectively, for CBC, resulting in a 5.8 times larger bending deformation than that of the pure CBC actuator. The developed high-performance CZ-PL muscular actuator can be a promising candidate for meeting the tight requirements of human-friendly electronic devices such as wearable devices, biomimetic robots, and biomedical active devices.

1. INTRODUCTION

Electroactive polymer (EAP) actuators have received great attention because of their biomimetic actuation, relatively large bending deformation, low operating voltage, flexibility, and relatively low cost [1–5]. Furthermore, high-performance EAP actuators with eco-friendly, biocompatible, and biodegradable functionalities have been considered to be promising candidates for human-friendly electronics, including wearable electronics, flexible haptic devices, smart mobile phones, braille displays, and biomedical devices [6–10]. To meet these requirements of green electronics, a promising method is to develop high-performance EAP actuators based on naturally abundant biopolymers such as cellulose acetate, silk, chitosan, plant cellulose, and bacterial cellulose. However, the cellulose-based EAP actuators exhibit relatively low actuation performance according to the open literature [11–16]. Therefore, the development of high-performance durable EAP actuators based on cellulose is highly desirable.

As a special kind of cellulose, bacterial cellulose (BC) is produced by several types of bacteria [17]. Although it has a molecular structure similar to that of natural cellulose, BC has higher purity and crystallinity, higher water holding capability and ionic exchange capacity (IEC), better mechanical properties, and no lignin or hemicellulose. BC is essentially composed of cellulose microfibrils with hydrogen bonding among the BC molecules, which are attributed to the presence of a large number of –OH radicals on the BC chains. These factors cause the BC fibers to aggregate and entangle tightly, resulting in a compound that is insoluble to all common solvents, including water. Therefore, BC-based electroactive soft actuators still exhibit low actuation performances due to their weak electrochemical activities [15,16,18].

Recently, many researchers have succeeded in the fabrication of homogenous BC dispersions by treating conventional BC using the 2,2,6,6-tetramethylpiperidine-l-oxyl radical (TEMPO)-mediated oxidation method [19–22]. The carboxylic groups are selectively oxidized on the surface of BC nanofibers, allowing the homogenous dispersion of individual BC nanofibers in water because of the electrostatic repulsion among the negatively charged carboxylate ions. These characteristics of the carboxylate BC (CBC) offer great potential for many applications, such as flexible films, strong materials, highly active nanohybrid catalysts,

* Corresponding authors.
E-mail addresses: jop@jnu.ac.kr (J.-O. Park), shpark12@dgist.ac.kr (S. Park).

http://dx.doi.org/10.1016/j.snb.2017.04.124
0925-4005/

and electrodes for energy devices [23,24]. More interesting, the carboxylic groups of CBC nanofibers can act as proton donators and ion exchange sites, and can greatly contribute to enhancements in the ionic liquid uptake and electrochemical activities. According to these unique properties, our group recently developed an ionic EAP actuator based on the CBC membrane and an ionic liquid, which showed better actuation performance than those of BC-based actuators [25]. However, the designed actuator still demonstrated relatively low actuation performance compared with other synthetic ionic EAP actuators because of lower IEC and ionic conductivity [25], which inspired us to further develop high-performance durable CBC-based actuators with superior electrochemical properties.

To achieve this goal, we newly fabricated porous CBC membranes using the zinc oxide (ZnO) particulate leaching (PL) method. The proposed CBC porous membrane demonstrated superior electro-chemo-mechanical properties with improved IEC and ionic conductivity, and tuned mechanical properties, which facilitated fast and easy ion transport inside the membrane matrix. In addition, ZnO is bio-safe and biocompatible, and can be used for biomedical applications [26,27]. This means that the use of ZnO does not affect the biological properties of BC. In this study, we developed a high-fidelity bioelectronic muscular actuator based on eco-friendly CBC porous membrane, flexible-nonmetallic conducting polymer poly(3,4-ethylenedioxythiopene)-polystyrenesulfonate (PEDOT:PSS) [28,29], and ionic liquid (1-Ethyl-3-methylimidazolium tetrafluoroborate, [EMIM][BF_4]) as a plasticizer [30–32], thereby achieving a high-performance actuator with a large bending deformation, low actuation voltage, quick response, and excellent actuation durability. The large bending deformation of this actuator was attributed to the enhanced electrochemical properties, tuned mechanical properties, and the electrochemical doping processes at the nonmetallic flexible PEDOT:PSS electrode layers. The total actuation mechanism of the actuator was due to the synergistic effects of the ion migration of ionic liquids within the porous CBC membrane and the electrochemical doping process of the PEDOT:PSS electrode layers.

2. EXPERIMENTAL SECTION

2.1. Preparation of the BC pellicles and CBC dispersions

The preparation process of the BC pellicles was reported in our previous works [16,18]. In brief, BC was cultivated using the Acetobacter xylinum KJ1 as the BC producer and the Glu-Fruc medium as the BC production medium. After incubating at 30 °C for 10 days, the BC pellicles were obtained from the BC production culture. The BC pellicles were then treated with sodium hydroxide solution (NaOH, 0.1 M) to lyse the bacteria and washed with deionized water several times.

CBC dispersions were prepared using the TEMPO-mediated oxidation method, according to our previous reports [24,25,33]. Briefly, BC pellicles (1.0 g) were suspended in 100 mL deionized water containing sodium bromide (NaBr, 0.1 g, 1 mM) and TEMPO (0.016 g, 0.1 mM) under gentle agitation at room temperature. Thereafter, sodium hypochlorite solution (12% NaClO, 3.1 g, 5.0 mM) was added to the suspension. The pH of the mixture was maintained at 10.5 by employing a 0.5 M sodium hydroxide (NaOH) solution. The oxidation reaction was quenched after 2 h. Then, the pH of the resulting suspension was adjusted to 7 by adding 0.5 M hydrochloric acid (HCl) solution. The CBC products were thoroughly filtered using deionized water. Finally, the CBC dispersion was obtained by adding 0.5 g of the CBC products into 100 mL deionized water under gentle stirring.

2.2. Preparation of the porous CZ-PL membranes

The porous CBC membranes were prepared using the PL method, as shown in Scheme 1. Zinc oxide nanoparticles (ZnO, 10 and 20 wt%, about 14 nm nanoparticle diameter) were added to the stable CBC dispersion (50 mg/10 ml), respectively, and were sonicated for 2 h to obtain homogenous dispersions. Then, the CBC-ZnO dispersions were poured into casting molds and dried at 65 °C for 10 h in a vacuum oven, when the CBC-ZnO (10 and 20 wt%) composite membranes were obtained. To remove the ZnO nanoparticles inside the membranes, the CBC-ZnO composite membranes were immersed in a 0.2 M HCl solution for 4 h. After these membranes were soaked in deionized water for 10 h and dried at 60 °C for 2 h in a vacuum oven, porous CBC membranes were finally obtained. In addition, the porous BC membranes were also fabricated by adding ZnO nanoparticles to the viscous and gel-like BC dispersions and then using the PL method. The as-prepared membranes, pure BC membrane, pure CBC membrane, CBC-ZnO (10 and 20 wt%) composite membranes, and BC-ZnO (10 and 20 wt%) and CBC-ZnO (10 and 20 wt%) composite membranes after PL method were denoted as BC, CBC, CZ10, CZ20, BZ10-PL, BZ20-PL, CZ10-PL, and CZ20-PL.

2.3. Preparation of the CZ-PL actuators

The CZ-PL actuators were fabricated by depositing highly conductive PEDOT:PSS layers on both the top and bottom surfaces of the CZ-PL membranes using a simple dip-coating method. To embed ionic liquids into membranes, the BC, BZ20-PL, CBC, CZ10-PL, and CZ20-PL membranes were soaked in the ionic liquid ([EMIM][BF_4]) for 12 h. After drying at 65 °C for 6 h in a vacuum

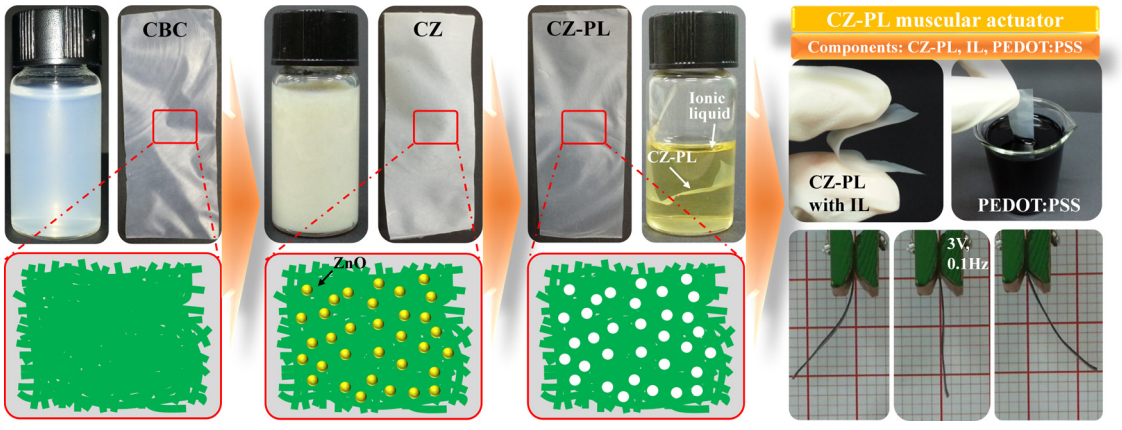

Scheme 1. Fabrication of the CZ-PL muscular actuator with the nonmetallic flexible PEDOT:PSS as an electrode.

oven, the membranes with absorbed ionic liquid were immersed into the PEDOT:PSS solution for 5 min; these membranes were then dried at 60 °C for 3 h in a vacuum oven. Finally, the CZ-PL actuators were obtained as shown in Scheme 1. The as-prepared actuators were cut to dimensions of 5 mm × 40 mm × 0.10 mm.

2.4. Materials characterization

Field emission scanning electron microscope (FE-SEM) images for the pure CBC, CZ20, and CZ20-PL membranes were recorded using a JSM-7500F (JEOL Co.). The Fourier transform-near-infrared (FT-IR) spectra were investigated using a FT-IR spectrometer (Spectrum 400, PerkinElmer Co.). To confirm the chemical compositions of the membrane samples, surface analysis was performed by employing a high resolution X-ray photoelectron spectroscopy (XPS) (ESCA, VG Multilab 2000 system, UK). X-ray diffraction (XRD) of the membranes was investigated using an X'Pert PRO multi-purpose diffractometer (PANalytical Co.). The surface area and pore size distribution were measured through the Brunauer-Emmett-Teller (BET) and Barrett-Joyner-Halenda (BJH) analyses using a surface area analyzer (ASAP2020, Micromeritics). The tensile strength and Young's modulus of the membranes were measured by a universal testing machine (AGS-X + 250, Shimadzu Corp.), and the testing speed was 10 mm min^{-1}. The membrane samples were cut into a rectangular shape and their cross-sectional areas were determined prior to testing with a micrometer. The gauge length between the grips was 10 mm. Three samples of a membrane were used for the mechanical test.

Ionic liquid (IL) uptake values were measured based on the mass difference between the dried samples and the samples with the absorbed ionic liquid. Ionic exchange capacity (IEC) of the membrane samples was determined from the conventional titration method. Three samples of a membrane with a fixed weight were immersed in 1 M NaCl solution for 24 h. Later, the solution was titrated using a 0.01 M NaOH solution. Finally, the IEC values were calculated using the following equation:

$$\text{IEC} = \frac{V_{\text{NaOH}}(\text{ml}) \times \text{molarity of NaOH}}{W} \quad (1)$$

where V_{NaOH} and W are the volume of NaOH and the weight of membranes, respectively.

The ionic conductivity of the membranes was determined using an impedance analyzer (VersaSTAT 3 potentiostat/galvanostat) over the frequency range 10 MHz to 100 Hz under a maximum voltage of 0.1 V. Three samples of a membrane of 1.0 cm × 1.0 cm size and an ECC-Std electrochemical cell were used. The ionic conductivities were determined according to the following equation: $\sigma = L/(R \times A)$, where σ (S cm^{-1}) is the ionic conductivity; L (cm) and A (cm^2) are the thickness and surface area of the membrane samples; R (Ω) is the ionic resistance, which is calculated from low-frequency intercept of the impedance with the real axis. The specific capacitances (F cm^{-2}) of the CZ-PL muscular actuators were determined from cyclic voltammetry CV) curves by using the following equation:

$$\text{Specific capacitance } (F\,\text{cm}^{-2}) = \frac{1}{\Delta V \cdot \nu \cdot S} \int_{V_1}^{V_2} IdV \quad (2)$$

where ΔV (V), ν (mV s^{-1}), and S (cm^2) are the potential window, scan rate, and surface area of the membrane samples, respectively. CV was carried out on a VersaSTAT 3 potentiostat/galvanostat with a two-electrode system.

2.5. Electromechanical characterization

The electromechanical responses including displacement and blocking force of the CZ-PL muscular actuators were tested by a laser displacement sensor (OFV-2510, Polytec Co.) and a load cell (TMO-2, Transducer Techniques Co.) in the test setups, which consisted of a DAQ (SCB-68, National Instruments), PXI 6252 data acquisition board, and current amplifier (UPM1503, Quanser), as shown in Fig. S1. All the data were obtained by an NI-PXI system by employing the LabView program. Actuators with a size of 5 mm × 40 mm were clamped at one end using about 5 mm × 5 mm area. The displacement (δ) of the actuator was measured at a position 5 mm away from the tip point. The free length (L) of the actuator was 30 mm. The measured displacement was transformed into the generated strain (ε) using the following equation [34]:

$$\varepsilon = \frac{2t \times \delta}{L^2 + \delta^2} \quad (3)$$

where δ, t, and L are the half of the peak to peak displacement, thickness, and free length of the actuator, respectively.

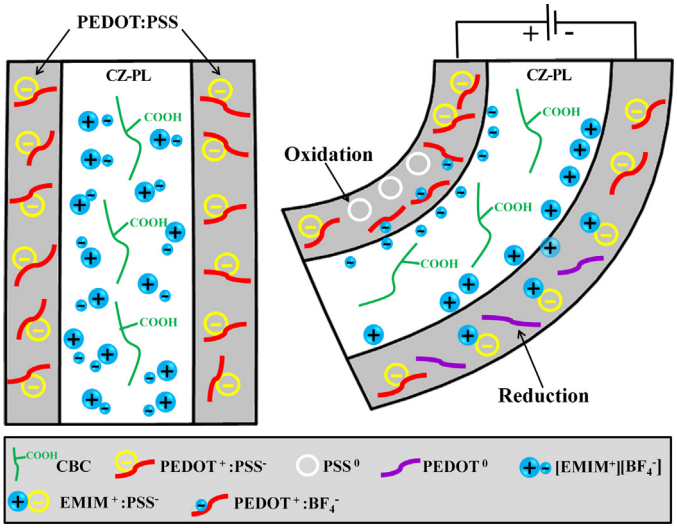

Fig. 1. Illustration of the actuation mechanism of the CZ-PL muscular actuator.

3. RESULTS AND DISCUSSION

3.1. Actuation mechanism

The structure of the CZ-PL actuator is shown in Fig. 1. There are three layers in the structure. The two out layers are the nonmetallic flexible PEDOT:PSS electrode layers and the middle layer is the CZ-PL membrane containing ionic liquid. The mechanism of actuation in conducting polymer actuators is known as doping/dedoping processes according to the electrochemical redox reaction [2,3,35]. Briefly, when an excitation voltage is applied to the PEDOT:PSS electrode layers, the potential difference between the electrode layers leads to the formation of PEDOT$^+$PSS$^-$ ion pairs by an electrochemical doping process and causes the absorption of the cations (i.e., EMIM$^+$) or anions (i.e., BF_4^-) of the ionic liquids into the electrode layer and to the ejection of counter ions from the other layer, as shown in Eqs. (1) and (2) [18,22,24]. Therefore, the bending deformation of the CZ-PL actuator is due to the differential expansion of the PEDOT:PSS electrode layer resulting from the electrochemical doping process of the PEDOT:PSS layer, and the bending direction is the same as the ionic migration within the CZ-PL membrane. In the anode electrode, the electrochemical reduction occurs as shown in Eq. (1). The PEDOT:PSS electrode layer consists of p-doped PEDOT$^+$ and PSS$^-$ oligomer chain. The PEDOT$^+$ networks provide the conduction path, and the PEDOT$^+$ is reduced to the neutral state (PSS^0) by the electron transfer into the PEDOT:PSS layer. Simultaneously, the dissociated cations (EMIM$^+$) obtained from ionic liquid

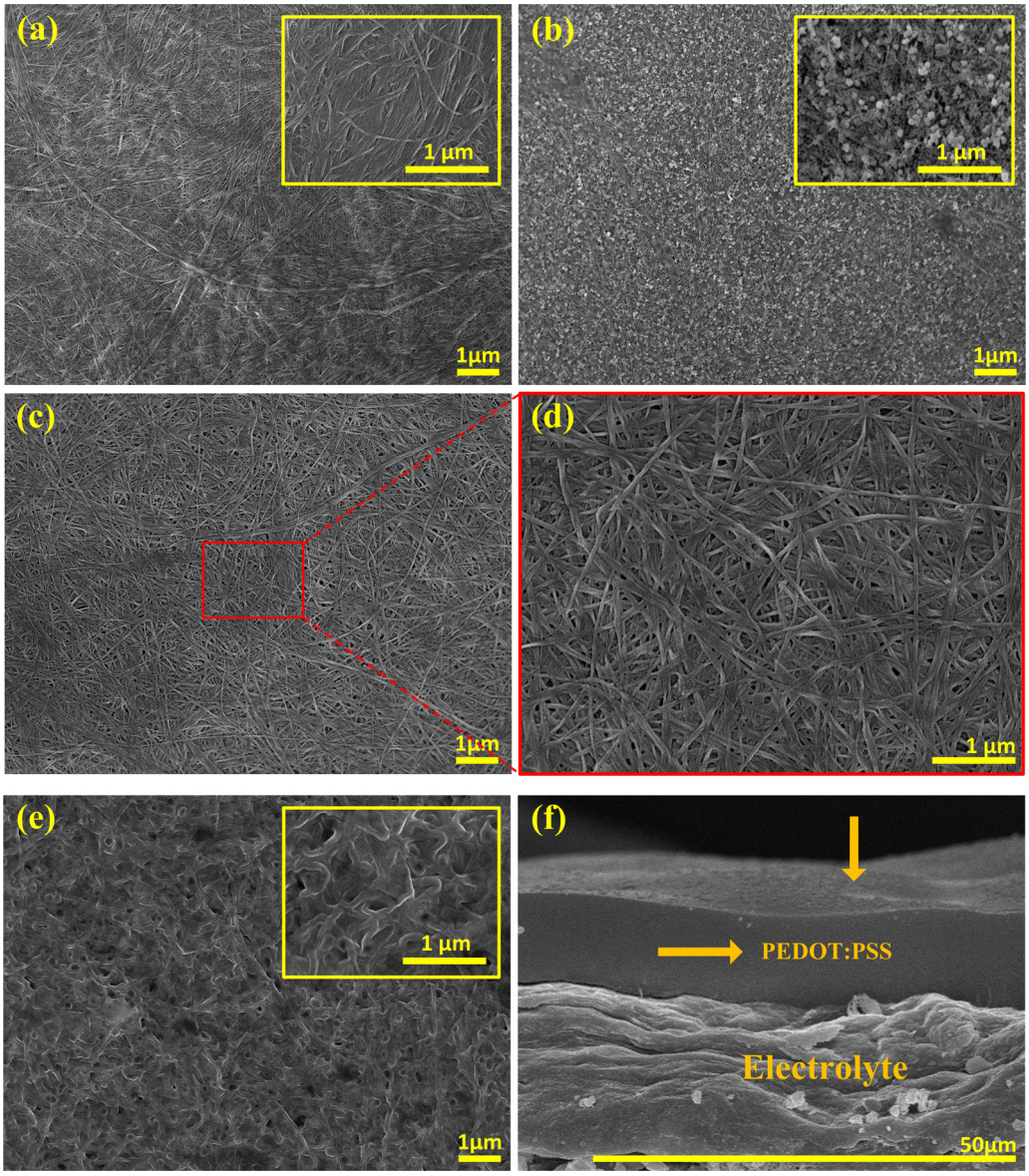

Fig. 2. FE-SEM images: (a–c) surface images of the pure CBC, CZ20, and CZ20-PL membranes, (d) magnified surface image of the CZ20-PL membrane, (e) surface image of the CZ20-PL membrane with ionic liquid, (f) cross-sectional image of the CZ20-PL muscular actuator.

([EMIM][BF_4]) engages in ionic bonding with PSS^-, which produce a large of quantity of swelling at the anode. Also, in the cathode electrode, the electrochemical oxidation occurs as shown Eq. (2). The anions (BF_4^-) obtained from ionic liquid bind ionically with $PEDOT^+$ cations. The PSS^- is oxidized to the neutral state (PSS^0) by anion injection into the PEDOT:PSS layer. Moreover, the molecular size of the anions (BF_4^-) is smaller than that of the cations ($EMIM^+$), indicating the bending direction of the actuation mechanism of the CZ-PL actuator. Thus, the total actuation mechanism of the actuator includes the electrochemical doping at the PEDOT:PSS layers and migration of ionic liquids inside the porous CZ-PL membrane under an electric field.

$$\begin{aligned} &PEDOT^{n+}: \quad PSS^{n-} + mEMIM^+ + me^- \leftrightarrow PEDOT^{(n-m)} \\ &+: \quad PSS^{(n-m)-} + mPEDOT^0 + m(EMIM^+: \quad PSS^-) \end{aligned} \tag{1}$$

$$\begin{aligned} &PEDOT^{n+}: \quad PSS^{n-} + mBF_4^- \quad PEDOT^{(n-m)+}: \quad PSS^{(n-m)^-} \\ &+mPSS^0 + m(PEDOT^+: BF_4^-) + me^- \end{aligned} \tag{2}$$

3.2. FE-SEM

FE-SEM was used to investigate the surface and cross-sectional morphologies of the pure CBC, CZ20, CZ20-PL, and CZ20-PL with ionic liquid, as shown in Fig. 2. The CBC membrane has a fibrous structure composed of ultrafine BC nanofibers (Fig. 1a). As shown in Fig. S2a, after TEMPO treatment, the characteristic peaks of CBC were the same as the pure BC. However, an absorption peak occurred at 1604^{-1}, indicating the presence of the carboxylic group in the bacterial cellulose. ZnO nanoparticles were clearly observed in the SEM images of CZ20 (Fig. 2b). As illustrated in Fig. 2c and 2d, the CZ20-PL membrane exhibited a highly porous structure in comparison with the pure CBC membrane, because the ZnO nanoparticles were dissolved by the PL method and changed into pores. The highly porous structure of the CZ20-PL membrane leads to superior electro-chemical properties such as improved IL uptake ratio, IEC, and ionic conductivity. As seen in Fig. 2e, the IL was dispersed well in the CZ20-PL membrane. The reasons include the

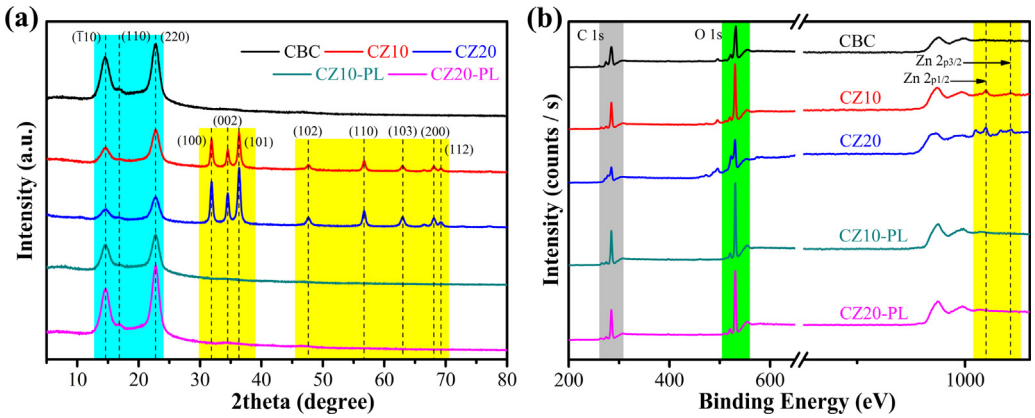

Fig. 3. (a) XRD curves and (b) XPS spectra of the pure CBC, CZ, and CZ-PL membranes.

following: i) hydrophilicity of the carboxylic groups of CZ20-PL; ii) ionic interaction between the IL and the carboxylic groups of CZ20-PL. Furthermore, the ionic interactions are confirmed by the FT-IR. One characteristic peak of the CZ20-PL membrane with IL appeared at the 1611 cm^{-1}, indicating the ionic interaction between the IL and carboxylic groups of the CZ20-PL, as seen in Fig. S2b. Fig. 2f shows the cross-sectional images of the CZ20-PL muscular actuator. The PEDOT:PSS electrode of this actuator is well bonded to the surface of CZ20-PL membrane without any delamination, which plays an important role in achieving high-performance durable ionic polymer actuators.

3.3. XRD and XPS

XRD results of the pure CBC, CZ, and CZ-PL membranes confirm that ZnO nanoparticles were clearly removed by using the PL method, as illustrated in Fig. 3a. The pure CBC membrane displayed three characteristic peaks at $2\theta = 14.6°$, 16.8°, and 22.7°, which were assigned to the $(1\bar{1}0)$, (110) and (220) diffraction planes of cellulose I, respectively [36]. The CZ10 and CZ20 membranes showed additional characteristic peaks at 2θ values of 31.8°, 34.6°, 36.3°, 47.5°, 56.7°, 63.1°, 68.2°, and 69.3° that were associated with the (100), (002), (101), (102), (110), (103), (200), and (112) diffraction planes, respectively, resulting from the addition of ZnO nanoparticles [37]. However, in the case of the CZ10-PL and CZ20-PL membranes, the characteristic peaks were the same as those of the pure CBC membrane, indicating that ZnO nanoparticles were completely removed through the PL method.

Furthermore, analyses of the XPS spectra prove that the ZnO nanoparticles in the CBC membranes could be removed using the PL method, as shown in Fig. 3b. The characteristic peaks of the pure CBC membrane appeared at 285.5 and 532 eV, which corresponded to C 1s and O 1s, respectively. Compared with the pure CBC membrane, the CZ10 and CZ20 membranes exhibited two additional peaks at 1019.5 and 1042 eV attributed to Zn $2p_{1/2}$ and Zn $2p_{3/2}$, respectively, indicating that ZnO nanoparticles were present in the CZ membranes [38]. For CZ10-PL and CZ20-PL membranes, there were no characteristic peaks of ZnO nanoparticles, which demonstrated that we could successfully remove ZnO nanoparticles using the PL method. Therefore, XRD and XPS analysis results verify that ZnO nanoparticles in the CBC membranes were completely removed by the PL method, and the CZ-PL membranes maintained the characteristic features of the CBC membranes.

3.4. Porosity

The porous structure of CZ20-PL membranes was studied using the BET and BJH analyses, as shown in Fig. 4. The CZ20-PL membrane exhibited the typical N_2 adsorption-desorption curve for porous materials (Fig. 4a). The surface area and total pore volume of the CZ20-PL membrane were found to be 45.18 $m^2\ g^{-1}$ and 0.21 $cm^3\ g^{-1}$, respectively; however, for the pure CBC membrane, the corresponding values were 3.29 $m^2\ g^{-1}$ and 0.01 $cm^3\ g^{-1}$, respectively [39]. The larger surface area and total pore volume of the CZ20-PL membrane compared to those of the pure CBC membrane were because the ZnO nanoparticles within the CZ20 membrane matrix were clearly removed using the PL method. In addition, there is a sharp N_2 uptake, indicating the well formation of meso- and macrospores. Furthermore, the pore size distributions of the pure CBC and CZ20-PL membranes are shown in Fig. 4b. It is

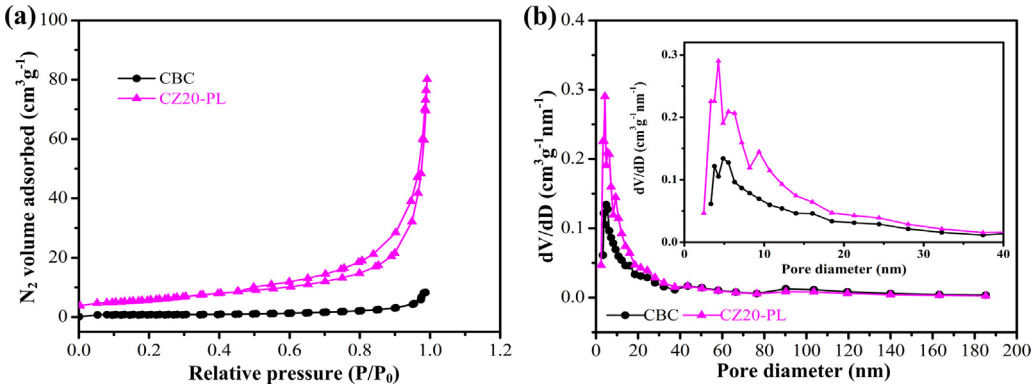

Fig. 4. (a) N_2 adsorption-desorption isotherms of the pure CBC and CZ20-PL membranes, (b) pore size distribution for the pure CBC and CZ20-PL membranes at 0–200 nm and 0–40 nm.

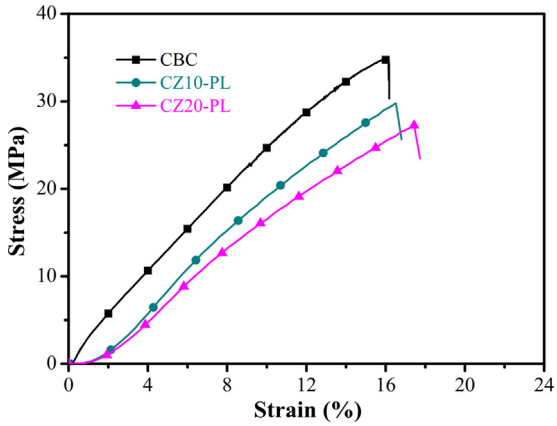

Fig. 5. Stress-strain curves of the pure CBC, CZ10-PL, and CZ20-PL membranes.

observed that the pore size distribution over the range between 4 and 40 nm increased. This is because the ZnO nanoparticles with different sizes were dissolved by the PL method. In addition, another reason for this pore size distribution may be attributed to ZnO nanoparticles not uniformly dispersed in the CBC membrane. The results of the porosity of the CZ20-PL membrane were consistent with those of the FE-SEM analysis. In addition, the highly porous structure of the CZ20-PL membrane facilitates ion transport within the membrane, thus leading to high-performance ionic polymer actuators.

3.5. Tensile test

The mechanical properties including the tensile strength and Young's modulus of the CZ-PL membranes have a significant effect on the actuation performance and the blocking force of the ionic polymer actuators. Fig. 5 shows the typical stress-strain curves of the pure CBC, CZ10-PL, and CZ20-PL membranes, and a comparison of their mechanical properties is shown in Table 1. According to Table 1, the tensile strength and Young's modulus of the pure CBC membrane were 34.61 MPa and 0.42 GPa, respectively, whereas they were 27.26 MPa and 0.32 GPa, respectively, for the CZ20-PL membrane. In particular, the proposed CZ20-PL membrane exhibited a superior elongation (up to 17.43%), which is better than that of the pure CBC membrane. These results demonstrate that the CZ20-PL membrane has a smaller tensile strength and Young's modulus than those of the pure CBC membrane. The main reason for this is attributed to the higher porous structure of the CZ20-PL membrane using the PL method. The lower stiffness of the proposed membrane is expected to enhance the bending deformation of the CZ20-PL actuators [16].

3.6. Electrochemical properties

The electrochemical properties of the membranes play a crucial role in evaluating the actuation performance of the ionic polymer actuators. Table 1 shows the electrochemical properties that include IL uptake ratio, IEC, and ionic conductivity of the pure CBC, CZ10-PL, and CZ20-PL membrane. As shown in Table 1, the IL uptake ratios of the three membranes were calculated to be 31.24% (CBC), 52.71% (CZ10-PL), and 70.63% (CZ20-PL), respectively. Among the three membranes, the CZ20-PL membrane had the highest IEC and ionic conductivity, up to 2.23 meq. g^{-1} and 2.08×10^{-3} S cm^{-1}, respectively. However, for the pure CBC membrane, the corresponding values are just 1.82 meq. g^{-1} and 1.76×10^{-3} S cm^{-1}, respectively. The experimental results indicate that the proposed CZ-PL membranes have enhanced electrochemical properties, such as IL uptake ratio, IEC, and ionic conductivity compared with the pure CBC membrane, resulting from the higher porous structure of the CZ-PL membranes. These characteristics can facilitate ion transport within the CZ-PL membranes, thus providing the capability of

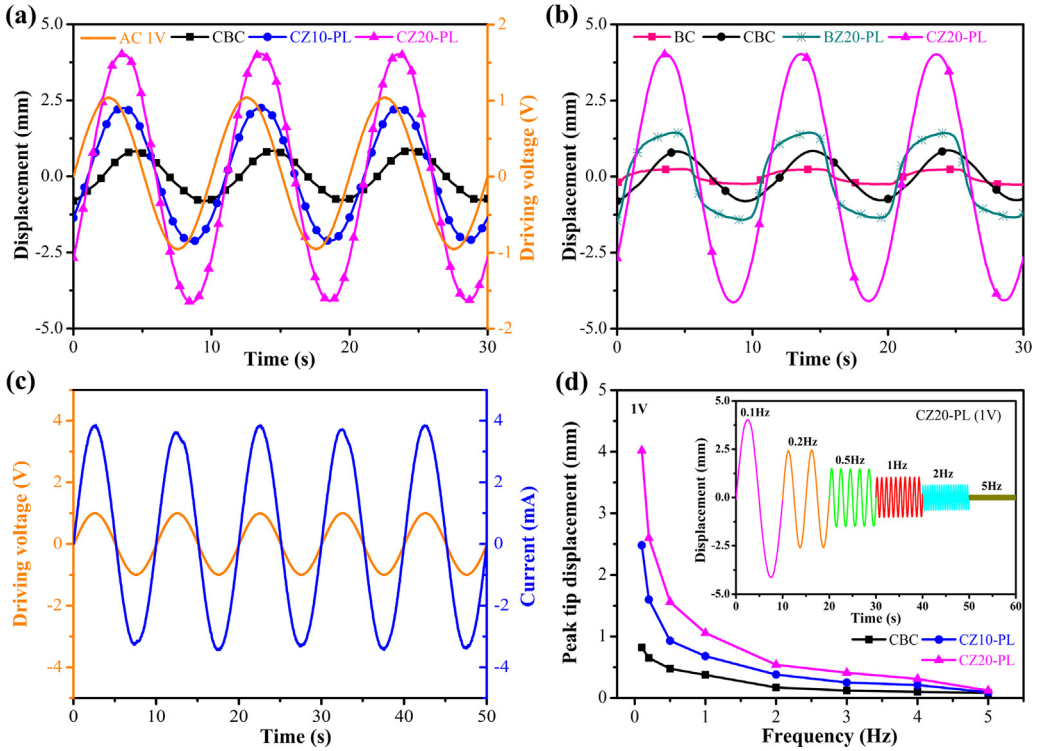

Fig. 6. Actuation performances of the CZ-PL muscular actuators: (a) harmonic responses under a sinusoidal excitation of 1.0 V at 0.1 Hz, (b) harmonic responses of the BC and BZ20-PL actuator under 1.0 V at 0.1 Hz, (c) current responses, (d) peak displacement under various frequencies.

Table 1
Electro-chemo-mechanical properties of the CZ-PL membranes.

Membrane	IL uptake ratio (%)	IEC [meq. g^{-1}]	Ionic conductivity [s cm^{-1}]	Young's modulus [GPa]	Tensile strength [Mpa]	Elongation at break [%]
BC	–	1.11 ± 0.01	$(7.90 \pm 0.07) \times 10^{-5}$	2.91 ± 0.12	274.12 ± 9.52	12.97 ± 0.14
CBC	31.24 ± 0.62	1.82 ± 0.02	$(1.76 \pm 0.03) \times 10^{-3}$	0.42 ± 0.06	34.61 ± 0.27	16.17 ± 0.04
CZ10-PL	52.71 ± 0.91	1.95 ± 0.02	$(1.93 \pm 0.02) \times 10^{-3}$	0.37 ± 0.03	29.80 ± 0.08	16.58 ± 0.07
CZ20-PL	70.63 ± 1.43	2.23 ± 0.03	$(2.08 \pm 0.04) \times 10^{-3}$	0.32 ± 0.04	27.26 ± 0.10	17.43 ± 0.06

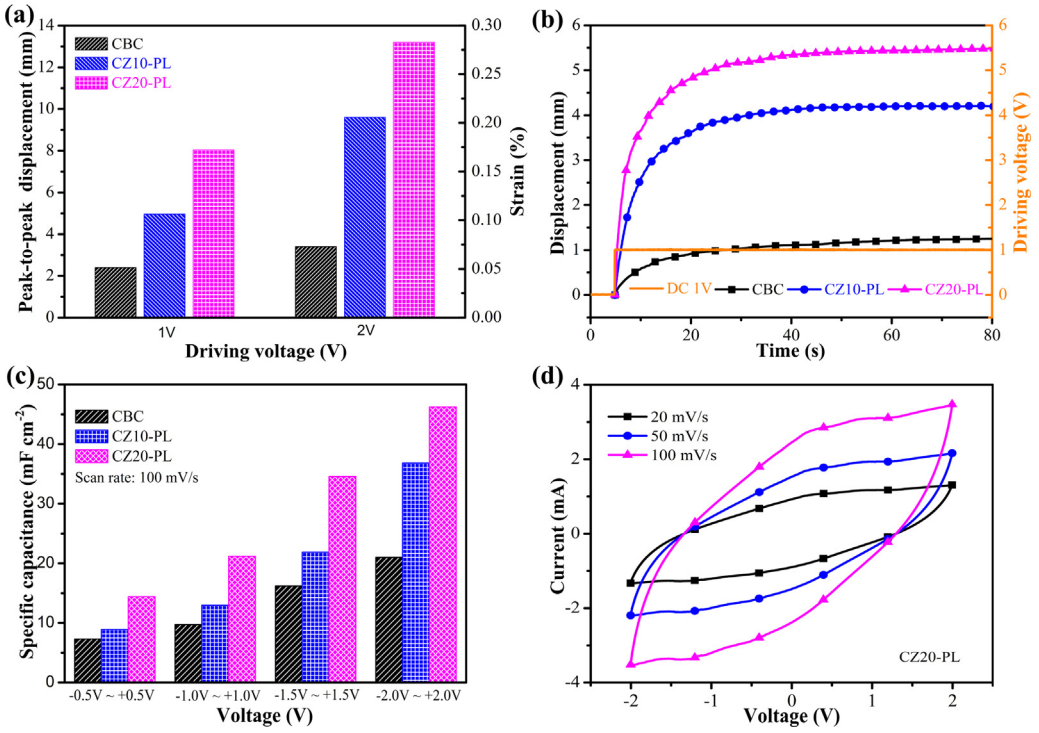

Fig. 7. (a) peak-to-peak displacement at different voltages and (b) step responses of the CZ-PL actuator, (c) specific capacitance of the CZ-PL actuator under various voltages at a scan rate of 100 mV s^{-1}, and (d) CV curves of the CZ-PL actuator under different scan rates.

improving the electromechanical performances of ionic polymer actuators.

3.7. Electromechanical performances

To evaluate the electromechanical performances of the CZ-PL muscular actuators in air, various electrical input signals were applied to their electrode layers. Fig. 6a shows the bending displacements of the actuators under sinusoidal voltages of ±1.0 V with a frequency of 0.1 Hz. The peak displacements of the CZ10-PL and CZ20-PL actuators were up to ±2.2 and ±4.1 mm, respectively, which were 3.14 times and 5.86 times than that of the CBC actuator (±0.7 mm). Also, the response times of the CZ-PL actuators were improved in comparison with those of the CBC actuator. As illustrated in Fig. 6b, the CBC actuator exhibited relatively larger displacement and faster response time compared with the pure BC actuator, which was due to the enhanced electro-chemical properties, resulting from the presence of the carboxylic groups in BC and the ionic interaction between IL and CBC. Also, the CZ20-PL actuator showed better actuation performances than those of the BZ20-PL actuator. The reason was mainly attributed to the CZ20-PL membrane having a highly porous structure with uniform pores. The highly porous structure facilitated ion transport within the membrane, thereby offering the capability to improve the bending actuation performances. Fig. 6c shows the current responses of the CZ20-PL actuator under a sinusoidal excitation of 1.0 V at 0.1 Hz, and the peak current of the actuator was 3.8 mA. These results demonstrate that the CZ-PL actuators show larger displacement and faster responses than those of the pure BC, CBC, and BZ-PL actuators, because of the higher IL uptake ratio, IEC, ionic conductivity, and lower stiffness of CZ-PL membranes obtained through the PL method. Moreover, the peak displacements of the actuators were investigated under different frequencies such as, 0.1, 0.2, 0.5, 1, 2, and 5 Hz, as shown in Fig. 6d. The actuation performances of the CZ-PL actuators were much higher compared to the CBC actuator at all frequencies. The inset graph in Fig. 6d exhibits the bending displacement of the CZ20-PL actuator at sinusoidal voltages of ±1.0 V with various excitation frequencies. The displacement of the actuator gradually increased as the excitation frequency decreased, which was attributed to the presence of ionic liquids inside the porous membrane that have sufficient time toward the electrode layers.

As seen in Fig. 7a, the peak-to-peak displacements and strains of the actuators were measured at sinusoidal voltages of ±1.0 V and ±2.0 V with a frequency of 0.1 Hz. The peak displacement and strain increased with the increment of the driving voltage. The actuation performance of the actuators was greatly affected by the driving voltage because of the high dependence of the mobility of the ionic liquids on the electric field inside the porous CZ-PL membrane. When the driving voltage was 2 V, the strain of the CZ20-PL actuator attained 0.28%, which is comparable to those of IL/polyurethane/PEDOT:PSS actuator [35], IL/PVDF/PEDOT:PSS actuator [40], and IL/carbon nanotube gel actuator [30]. Fig. 7b shows the displacements of the actuators under a DC excitation of

1.0 V. The maximum displacements of the CBC, CZ10-PL and CZ20-PL actuators were 1.3, 4.2, and 5.4 mm, respectively, without the presence of the back-relaxation phenomenon which is attributed to the weakly polar carboxylic groups in the CBC matrix. The enhanced bending displacements of the proposed CZ-PL actuator were because of its superior electro-chemo-mechanical properties. Furthermore, Fig. 7c and 7d exhibit the specific capacitance and cyclic voltammetric (CV) of CZ-PL muscular actuators, respectively. The measured specific capacitances of the CZ20-PL (46.25 mF cm^{-2}) and CZ10-PL (36.83 mF cm^{-2}) actuators are larger than that of the pure CBC (21 mF cm^{-2}) actuator under ±2.0 V peaks at a scan rate of 100 mV s^{-1} (Fig. 7c). The larger specific capacitance means a better charge accumulation and has an important role in realizing an enhanced bending deformation of ionic polymer actuators. As seen in Fig. 7d, the CV tests of the CZ20-PL actuator were performed under various scan rates. The roughly rectangular shape of the CV curve, i.e., capacitive hysteresis behavior, means the good charge propagation within the porous CZ20-PL membrane.

Fig. 8a shows the optical images of the CZ20-PL actuator under a sinusoidal voltage of 3.0 V with a frequency of 0.1 Hz. The actuator showed a large and symmetrical bending deformation according to the sinusoidal voltage. Fig. 8b shows the large deformed shapes of the CZ20-PL actuator under a DC excitation of 2.0 V without the presence of the back-relaxation phenomenon. A relatively high performance and fast response of the muscular actuator were observed. Also, the bending deformation of the actuator was steady under the quasi-static excitation because of the effective migration of ionic liquids inside the porous CZ-PL membrane. We found that the CZ-PL muscular actuator showed a larger bending deformation and faster response under various harmonic and step excitations than those of the pure CBC actuator. The improved actuation performance of the proposed CZ-PL actuator was because of its higher IL uptake ratio, IEC, and ionic conductivity, and lower stiffness, all of which resulted from the highly porous CZ-PL membrane by the PL method. The actuation mechanism of the CZ-PL muscular actuator was due to the synergistic effects of the electrochemical doping at the PEDOT:PSS layers and migration of ionic liquids inside the porous CZ-PL membrane under an electric field [24,25,39].

In addition, the actuation durability of the CZ20-PL muscular actuator was evaluated under a sinusoidal voltage of ±1.0 V with a frequency of 0.1 Hz, as illustrated in Fig. 9a. We found that this actuator demonstrated a durable actuation performance without an apparent decrease in the bending displacement during a sinusoidal excitation for 120 min. The excellent actuation durability of the CZ20-PL actuator was attributed to its superior electro-chemo-mechanical properties and the electrochemical doping at the PEDOT:PSS layers. In addition, Fig. 9b shows the blocking force of the three actuators under a DC voltage of 2.0 V. The CZ20-PL actuator demonstrated the highest blocking force, which was 1.72 times more than that of the CBC actuator.

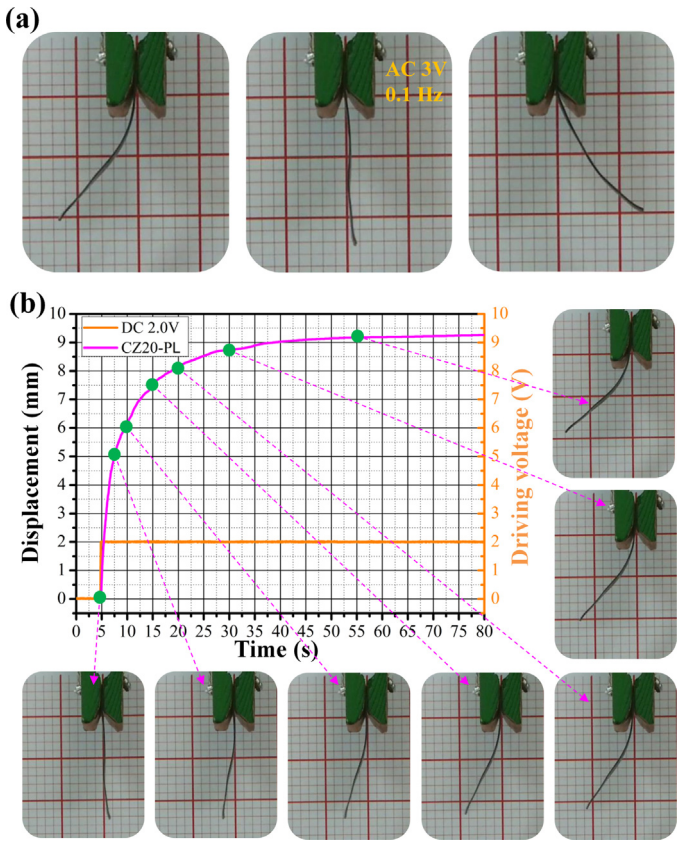

Fig. 8. Electromechanically deformed shapes of the CZ20-PL muscular actuator under (a) a sinusoidal excitation of 3.0 V at 0.1 Hz and (b) a step excitation of 2.0 V.

4. CONCLUSIONS

In summary, we have demonstrated a novel high-performance durable muscular actuator, so called CZ-PL actuator, based on porous CBC membrane, ionic liquid, and PEDOT:PSS electrode, leading to superior electro-chemo-mechanical properties and actuation performances. The proposed CZ20-PL membranes exhibited an increased IL uptake ratio, IEC, and ionic conductivity of up to 70.63%, 22.5%, and 18.2%, respectively, which facilitated easy and fast ion transport within the membrane matrix, and therefore resulted in CZ20-PL muscular actuators with large deformation, fast response, low-actuation voltage, and high-durability. More-

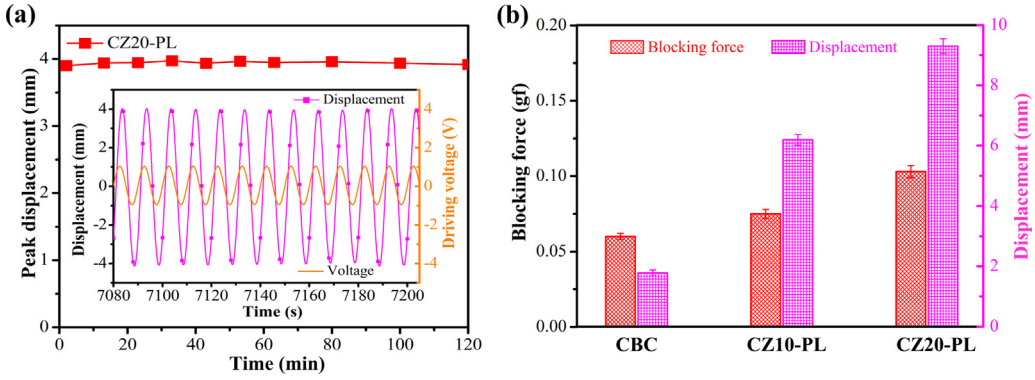

Fig. 9. (a) Actuation durability of the CZ20-PL muscular actuator under a sinusoidal excitation of 1.0 V at 0.1 Hz, (b) blocking force of the CBC and CZ20-PL actuator.

over, all used materials are naturally abundant, eco-friendly, and low cost, thus these CZ-PL muscular actuators can be promising candidates for wearable electronics, soft haptic devices, biomimetic robots, and implantable or disposal biomedical devices that require high-performance electroactive soft actuators with eco-friendly, biocompatible, and biodegradable functionalities.

Acknowledgments

This research was supported by the Next-generation Medical Device Development Program for Newly-Created Market of the National Research Foundation (NRF) funded by the Korean government, MSIP (No.2015M3D5A1065682).

Appendix A. Supplementary data

Supplementary data associated with this article can be found, in the online version, at http://dx.doi.org/10.1016/j.snb.2017.04.124.

References

[1] M. Shahinpoor, Y. Bar-Cohen, J.O. Simpson, J. Smith, Ionic polymer-metal composites (IPMCs) as biomimetic sensors, actuators and artificial Muscles – a review, Smart Mater. Struct. 7 (1998) R15.
[2] E. Smela, Conjugated polymer actuators for biomedical applications, Adv. Mater. 15 (2003) 481–494.
[3] T.F. Otero, M.T. Cortés, A sensing muscle, Sens. Actuators B 196 (2003) 152–156.
[4] S. Hara, T. Zama, W. Takashima, K. Kaneto, TFSI-doped polypyrrole actuator with 26% strain, J. Mater. Chem. 14 (2004) 1516–1517.
[5] T. Sugino, K. Kiyohara, I. Takeuchi, K. Mukai, K. Asaka, Actuator properties of the complexes composed by carbon nanotube and ionic liquid: the effects of additives, Sens. Actuators B 141 (2009) 179–186.
[6] R.H. Baughman, Playing nature's game with artificial muscles, Science 308 (2005) 63–65.
[7] J. Kim, S. Yun, Discovery of cellulose as a smart material, Macromolecules 39 (2006) 4202–4206.
[8] C. Jo, D. Pugal, I.K. Oh, K.J. Kim, K. Asaka, Recent advances in ionic polymer–metal composite actuators and their modeling and applications, Prog. Polym. Sci. 38 (2013) 1037–1066.
[9] L. Lu, W. Chen, Biocompatible composite actuator: a supramolecular structure consisting of the biopolymer chitosan, carbon nanotubes, and an ionic liquid, Adv. Mater. 22 (2010) 3745–3748.
[10] N. Terasawa, K. Asaka, High-performance polymer actuators based on an iridium oxide and vapor-grown carbon nanofibers combining electrostatic double-layer and faradaic capacitor mechanisms, Sens. Actuators B 240 (2017) 536–542.
[11] J. Li, S. Vadahanambi, C.D. Kee, I.K. Oh, Electrospun fullerenol-cellulose biocompatible actuators, Biomacromolecules 12 (2011) 2048–2054.
[12] G.M. Spinks, S.R. Shin, G.G. Wallace, P.G. Whitten, I.Y. Kim, S.I. Kim, S.J. Kim, A novel "dual mode" actuation in chitosan/polyaniline/carbon nanotube fibers, Sens. Actuators B 121 (2007) 616–621.
[13] I.S. Romero, N.P. Bradshaw, J.D. Larson, S.Y. Severt, S.J. Roberts, M.L. Schiller, J.M. Leger, A.R. Murphy, Biocompatible electromechanical actuators composed of silk-conducting polymer composites, Adv. Funct. Mater. 24 (2014) 3866–3873.
[14] J. Li, W. Ma, L. Song, Z. Niu, L. Cai, Q. Zeng, X. Zhang, H. Dong, D. Zhao, W. Zhou, S. Xie, Superfast-response and ultrahigh-power-density electromechanical actuators based on hierarchal carbon nanotube electrodes and chitosan, Nano lett. 11 (2011) 4636–4641.
[15] J. Kim, Y.B. Seo, Electro-active paper actuators, Smart Mater. Struct. 11 (2002) 355.
[16] J.H. Jeon, I.K. Oh, C.D. Kee, S.J. Kim, Bacterial cellulose actuator with electrically driven bending deformation in hydrated condition, Sens. Actuators B 146 (1) (2010) 307–313.
[17] M. Iguchi, S. Yamanaka, A. Budhiono, Bacterial cellulose-a masterpiece of nature's arts, J. Mater. Sci. 35 (2000) 261–270.
[18] S.S. Kim, J.H. Jeon, C.D. Kee, I.K. Oh, Electro-active hybrid actuators based on freeze-dried bacterial cellulose and PEDOT: PSS, Smart Mater. Struct. 22 (2013) 085026.
[19] A. Isogai, T. Saito, H. Fukuzumi, TEMPO-oxidized cellulose nanofibers, Nanoscale 3 (2011) 71–85.
[20] Z. Fang, H. Zhu, Y. Yuan, D. Ha, S. Zhu, C. Preston, Q. Chen, Y. Li, X. Han, S. Lee, G. Chen, T. Li, J. Munday, J. Huang, L. Hu, Novel nanostructured paper with ultrahigh transparency and ultrahigh haze for solar cells, Nano lett. 14 (2014) 765–773.
[21] F. Wang, H.J. Kim, S. Park, C.D. Kee, S.J. Kim, I.K. Oh, Bendable and flexible supercapacitor based on polypyrrole-coated bacterial cellulose core-shell composite network, Compos. Sci. Technol. 128 (2016) 33–40.
[22] F. Wang, J.H. Jeon, S.J. Kim, J.O. Park, S. Park, An eco-friendly ultra-high performance ionic artificial muscle based on poly (2-acrylamido-2-methyl-1-propanesulfonic acid) and carboxylated bacterial cellulose, J. Mater. Chem. B 4 (2016) 5015–5024.
[23] H. Koga, T. Saito, T. Kitaoka, M. Nogi, K. Suganuma, A. Isogai, Transparent, conductive, and printable composites consisting of TEMPO-oxidized nanocellulose and carbon nanotube, Biomacromolecules 14 (2013) 1160–1165.
[24] S.S. Kim, J.H. Jeon, H. Kim, C.D. Kee, I.K. Oh, High-Fidelity Bioelectronic Muscular Actuator Based on Graphene-Mediated and TEMPO-Oxidized Bacterial Cellulose, Adv. Funct. Mater. 25 (2015) 3560–3570.
[25] F. Wang, J.H. Jeon, S. Park, C.D. Kee, S.J. Kim, I.K. Oh, A soft biomolecule actuator based on a highly functionalized bacterial cellulose nano-fiber network with carboxylic acid groups, Soft Matter 12 (2016) 246–254.
[26] Z.L. Wang, Nanostructures of zinc oxide, Mater. Today 7 (2004) 26–33.
[27] Y.Q. Fu, J.K. Luo, X.Y. Du, A.J. Flewitt, Y. Li, G.H. Markx, A.J. Walton, W.I. Milne, Recent developments on ZnO films for acoustic wave based bio-sensing and microfluidic applications: a review, Sens. Actuators B 143 (2010) 606–619.
[28] A. Simaite, F. Mesnilgrente, B. Tondu, P. Souères, C. Bergaud, Towards inkjet printable conducting polymer artificial muscles, Sens. Actuators B 229 (2016) 425–433.
[29] J.H. Jeon, R.K. Cheedarala, C.D. Kee, I.K. Oh, Dry-type artificial muscles based on pendent sulfonated chitosan and functionalized graphene oxide for greatly enhanced ionic interactions and mechanical stiffness, Adv. Funct. Mater. 23 (2013) 6007–6018.
[30] N. Terasawa, K. Mukai, K. Asaka, Improved performance of an active multi-walled carbon nanotube polymer actuator, compared with a single-walled carbon nanotube polymer actuator, Sens. Actuators B 173 (2012) 66–71.
[31] N. Terasawa, K. Asaka, High-performance PEDOT:PSS/single-walled carbon nanotube/ionic liquid actuators combining electrostatic double-layer and faradaic capacitors, Langmuir 32 (2016) 7210–7218.
[32] L. Wei, G. Yushin, Electrical double layer capacitors with sucrose derived carbon electrodes in ionic liquid electrolytes, J. Power. Sources 196 (2011) 4072–4079.
[33] F. Wang, S.S. Kim, C.D. Kee, Y.D. Shen, I.K. Oh, Novel electroactive PVA-TOCN actuator that is extremely sensitive to low electrical inputs, Smart. Mater. Struct. 23 (2014) 074006.
[34] L. Kong, W. Chen, Carbon Nanotube and Graphene-based Bioinspired Electrochemical Actuators, Adv. Mater. 26 (2014) 1025–1043.
[35] H. Okuzaki, S. Takagi, F. Hishiki, R. Tanigawa, Ionic liquid/polyurethane/PEDOT: PSS composites for electro-active polymer actuators, Sens. Actuators B 194 (2014) 59–63.
[36] T. Maneerung, S. Tokura, R. Rujiravanit, Impregnation of silver nanoparticles into bacterial cellulose for antimicrobial wound dressing, Carbohydrate Polym. 72 (2008) 43–51.
[37] C. Pacholski, A. Kornowski, H. Weller, Self-assembly of ZnO: from nanodots to nanorods, Angew. Chem. Int. Ed. 41 (2002) 1188–1191.
[38] X.Q. Wei, B.Y. Man, M. Liu, C.S. Xue, H.Z. Zhuang, C. Yang, Blue luminescent centers and microstructural evaluation by XPS and Raman in ZnO thin films annealed in vacuum, N_2 and O_2, Physica B. 388 (2007) 145–152.
[39] D. Sun, J. Yang, X. Wang, Bacterial cellulose/TiO2 hybrid nanofibers prepared by the surface hydrolysis method with molecular precision, Nanoscale 2 (2010) 287–292.
[40] A. Simaite, B. Tondu, P. Souères, C. Bergaud, Hybrid PVDF/PVDF-graft-PEGMA membranes for improved interface strength and life time of the PEDOT:PSS/PVDF/Ionic liquid actuators, ACS Appl. Mater. Interfaces 7 (2015) 19966–19977.

Biographies

Fan Wang completed his MS in mechanical engineering at Chonnam National University, Korea in 2013. He is currently in a doctoral course in the Department of Mechanical Engineering at Chonnam national University. He has interests in electroactive Polymer, artificial muscles, flexible electronics, and energy storage.

Zhen Jin obtained his B.S. (2012) degree from the department of Mechanical Engineering at Yanbian University of Science and Technology (YUST), China. Currently, he is a Ph.D. candidate in Chonnam National University and a researcher in Robot Research Initiative. His research interests are micro/nanorobots, high focused ultrasound (HIFU), and drug delivery system.

Shaohui Zheng earned his Master's degree in Mechanical Engineering from Chonnam National University, Korea in 2014. He continued his Ph.D. course in the Robot Research Initiative of Chonnam National University in 2014. He is carrying out the research about development of hyaluronic acid nanoparticles and bacteria based microrobots.

Hao Li obtained his B.S. (2011) degree from the department of Mechanical Engineering at Yanbian University of Science and Technology (YUST), China. Currently, he is a Ph.D. candidate in Chonnam National University and a researcher in Medical Microrobot Center (MRC). His research interests are hydrogel actuator, Bio-printing, and drug delivery system.

Sunghoon Cho completed his MS in Particle Physics from the Chonnam National University in 2011. He joined the "Super-Kamiokande" of the "Institute for Cosmic Ray Research. University of Tokyo" (ICRR) in 2010. In the School of Mechanical Engineering, Chonnam National University, he is working on the computational modeling of microrobot and development of functional micro/nanoparticles.

Hyeon Joe Kim completed his MS in Environmental engineering at Chonnam National University, Korea in 2014. He is currently in a doctoral course in the Department of Environmental and Energy Engineering at Chonnam national University.

Seong-Jun Kim graduated from the Tokyo Institute of Technology in 1998, receiving his PhD in Chemical Engineering. He joined the Department of Environmental Engineering as a faculty member at Chonnam National University in 1999. His research interests include Pilot-scale production of bacterial cellulose and Scale-up analysis.

Eunpyo Choi earned his Master's degree (2010) and Ph.D. (2015) in Mechanical Engineering from Sogang University, Korea. From 2015 to 2016, he worked as a senior Post-Doctoral Fellow in Bioengineering from University of Washington. In 2017, he joined the School of Mechanical Engineering as a faculty at Chonnam National University. His research interests are micro/nano medical robots, micro/nanofluidics, bioMEMS, biosensors, micro/nanofabrication.

Jong-Oh Park received his Master's degree in Mechanical Engineering from Korea Advanced Institute of Science and Technology (KAIST), Korea in 1981 and Dr.-Ing in Robotics from Stuttgart University, Germany in 1987. From 1982 to 1987, he worked as a guest researcher Fraunhofer-Gesellschaft Institut fur Produktions technik und Automatisierung (FhG IPA), Germany. He worked as a principal researcher in the Korea Institute of Science and Technology (KIST) from 1987 to 2005, and he was a director of the Microsystem Research Center in KIST from 1999 to 2005. In 2005, he moved to Chonnam National University, where he is now a professor of the School of Mechanical Engineering and a director of the Medical Microrobot Center (MRC). His research interests are biomedical microrobot, medical robot and service robot.

Sukho Park earned his Master's degree (1995) and Ph.D. (2000) in Mechanical Engineering from Korea Advanced Institute of Science and Technology (KAIST), Korea. From 2000 to 2004, he worked as a senior research engineer at LG Electronics Production Research Center, Korea. From 2004 to 2006, he worked as a senior researcher of Microsystem Research Center in the Korea Institute of Science and Technology. From 2006 to 2016, he worked as a professor of the School of Mechanical Engineering in Chonnam National University and a section head of the robot research initiative (RRI). In 2017, he moved to Daegu Gyeongbuk Institute of Science and Technology (DGIST), where he is now a full professor in Department of Robotics Engineering. His research interests are microactuator/robot and micromanipulation for biomedical instrumental applications.